Solar Energy Materials & Solar Cells 157 (2016) 1048–1056

Contents lists available at ScienceDirect

Solar Energy Materials & Solar Cells

journal homepage: www.elsevier.com/locate/solmat

Atmospheric growth of hybrid ZnO thin films for inverted polymer solar cells

Chandan Biswas [a], Zhu Ma [a,b], Xiaodan Zhu [a], Toshiyuki Kawaharamura [c], Kang L. Wang [a,*]

[a] Department of Electrical Engineering, Department of Materials Science & Engineering, Center of Excellence for Green Nanotechnologies, University of California, Los Angeles, CA 90095, USA
[b] School of Optoelectronic Information, University of Electronic Science and Technology of China, Chengdu 610054, China
[c] Research Institute, School of System Engineering, Kochi University of Technology, Kami, Kochi 7828502, Japan

ARTICLE INFO

Article history:
Received 17 May 2016
Received in revised form
26 July 2016
Accepted 22 August 2016
Available online 4 September 2016

Keywords:
Mist-CVD
Hybrid ZnO film
Atmospheric growth
Inverted polymer solar cells

ABSTRACT

Thin oxide materials are increasingly gaining popularity as both active and passive components for flexible and transparent electronic devices. Synthesis methods play crucial role for optimal electronic and optoelectronic properties. Conventional thin film growth methods primarily employ high energy-consumption processes such as ultra-high vacuum and high-temperature operations. Low energy-consumption synthesis processes became critically important for large scale applications. Here we show a novel approach to synthesize hybrid ZnO thin film using a combination of mist chemical vapor deposition and sol-gel techniques under atmospheric pressure conditions. The resulting hybrid ZnO thin films exhibit significant improvements in inverted polymer solar cell (IPSC). The performance improvements include carrier concentrations up to 1.5×10^{16} cm^{-3}, carrier lifetimes of 4×10^{-6} sec, and mobility up to 0.032 cm^2/Vs in hybrid ZnO based IPSC devices. A 36% increase in the power conversion efficiency (PCE from 3.1% to 4.23%) was observed utilizing the hybrid ZnO layer compared to their non-hybrid counterparts. These results highlight a simple and inexpensive alternative to produce hybrid ZnO layer with mass production compatibility for highly improved polymer solar cell applications.

1. Introduction

Wide bandgap oxide semiconductors are emerging as dominant players for electronic and optoelectronic applications [1]. Thin films and nanostructured oxides are increasingly gaining popularity as passive and active components, particularly in the field of flexible and transparent devices. Oxides of different origins play important roles in device operation, increasingly becoming more viable alternatives to conventional semiconductors. Synthesis methods play crucial roles controlling electronic and optoelectronic properties of the oxide materials. Conventional thin-film growth methods mostly contain high energy consumption processes such as high temperature and/or ultra-high vacuum processing. Energy consumption can be significantly reduced by using a method which is less dependent on ultra-high vacuum processing.

Low energy consumption, low environmental load, simple configuration, easy and inexpensive maintenance are among the advantages of a non-vacuum system. However, precise control of atmosphere and temperature are required for high-quality oxide material growth at atmospheric pressure. Here we show a novel approach to synthesize oxide materials (such as zinc oxide) under atmospheric conditions by a mist chemical vapor deposition (mist-CVD) technique. In recent years, various approaches to grow or deposit ZnO thin films have been used extensively. Pulsed laser deposition (PLD), molecular beam epitaxy (MBE), magnetron sputtering, metal-organic chemical vapor deposition (MOCVD), chemical vapor deposition (CVD), as well as solution-based approaches such as hydrothermal, sol-gel, electrochemical deposition are among the conventional ZnO synthesis approaches [2–7]. Magnetron sputtering and solution-based approaches typically yield polycrystalline films. On the other hand, PLD, MBE and MOCVD can produce high-quality mono-crystalline or epitaxial films. These techniques are complicated and expensive. The mist-CVD process is simple, inexpensive, and can yield high quality films at low temperatures. It is a combination of spray pyrolysis and CVD methods which allows the deposition to occur in the vapor phase [8–14]. The precursor mist was introduced by spraying through a well-defined temperature profile result in the formation of a thin film on the substrate surface. Furthermore, the atmospheric operation condition of mist-CVD enables the use of

* Corresponding author.
E-mail address: wang@ee.ucla.edu (K.L. Wang).

http://dx.doi.org/10.1016/j.solmat.2016.08.022
0927-0248/

varieties of environment friendly solvents (such as water), with clear mass-production potentials.

ZnO is a promising candidate for n-type carrier conduction in polymer solar cell structures due to its relatively high electron mobility, environmental stability, and high transparency [15]. ZnO thin film is a heavily used material for a broad range of solar cell applications such as organic polymer solar cell, dye sensitized solar cell, quantum dot solar cell. The hybrid-ZnO layers could be a strong candidate to replace existing ZnO materials for higher solar cell device performances. However, their efficiencies are often limited by low ZnO carrier mobility and the typically rough surface morphologies as reported previously [15,16]. An effective strategy for ZnO thin film synthesis with high carrier concentration, high carrier mobility and large scale uniformity is critical for high efficiency solar cell devices. In this work, we show a novel strategy to synthesize high quality hybrid ZnO thin films for inverted polymer solar cells with high carrier mobility, carrier concentration, and large scale uniformity. Hybrid ZnO thin films were synthesized by simple, inexpensive approach with large scale synthesis compatibilities using a combination of mist-CVD and sol-gel processes. The growth of the hybrid ZnO layer was optimized in order to maximize solar cell carrier concentration, mobility and subsequent device efficiency. The details of these improvements were analyzed in depth by evaluating the large scale surface roughness, carrier concentration, carrier mobility, device carrier lifetime and other device parameters. Our results show that the atmospheric process can be used for achieving high quality hybrid ZnO thin films, and could be applicable for polymer solar cell, dye sensitized solar cell, quantum dot solar cell and other optoelectronic devices.

2. Materials and methods

2.1. Mist-CVD ZnO layer synthesis

A custom made mist assisted chemical vapor deposition system (Fig. 1a) was used for ZnO thin film synthesis. The system consists of two main chambers, i) mist generation chamber and ii) a sample reaction chamber. Zinc acetate dihydrate (Sigma Aldrich, 99.9%) was dispersed in deionized water with a concentration of 0.025 M and stirred for 1 h. A solution of 0.027 vol% acetic acid (Sigma Aldrich) was added during the stirring process to enhance solute dissolution rate. This precursor solution was then transferred into the mist generation chamber. An ultrasonic transducer (BEANS International Corp.) was employed to generate mist vapor inside the chamber before transferring them into the sample reaction chamber for ZnO synthesis on top of a heated substrate.

2.2. Hybrid ZnO thin film synthesis

One gram of zinc acetate dihydrate and 0.28 g of ethanolamine (Sigma Aldrich, 99.5%) was dissolved in 2-methoxyethanol (Sigma Aldrich, 99.8%) and stirred for 12 h in air. This solution was then spin coated on top of the mist-CVD grown ZnO film with 4000 rpm for 40 s. A vacuum annealing procedure was conducted in order to finalize the hybrid ZnO layer. In this process the spin coated sample was placed into a vacuum oven while reducing the chamber pressure to lower than 1 mbar range. The sample was heated to 200 °C in the course of 30 min and kept under a constant temperature conditions for additional 60 min.

2.3. IPSC device fabrication

Commercially available P3HT:PCBM (1:1 wt-ratio) was dispersed in dichlorobenzene solvent at a concentration of 20 mg/mL and stirred for 14 h inside a nitrogen filled glove box. The mixture was kept at a constant temperature of 35 °C for 10 h and increased to 40 °C during last 4 h of the dispersion process. The P3HT:PCBM mixture was then spin coated on top of the hybrid ZnO coated ITO/glass substrate at 600 rpm for 20 s followed by 1100 rpm for 9 s. A 150 °C annealing for 5 min was conducted before the thermal deposition of the 10 nm molybdenum trioxide (MoO_3) and 100 nm silver (Ag) layers.

2.4. Device characterizations

J-V characteristics were measured using a Keithley 2400 source meter. AM 1.5 solar illumination was generated by using an Oriel Xenon lamp with appropriate optical filters. AFM measurements were conducted using a SPA 300 HV, Seiko Instrument Inc. system. Field emission scanning electron micrographs were obtained from a JEOL JSM-6700F FE-SEM system. Transmittance spectra were obtained by using a UV–Vis spectroscopy system (Ocean Optics, USB2000+UV–Vis). C-V measurements and impedance measurements were conducted with Agilent 4294A Precision Impedance Analyzer.

3. Results and discussion

Precise control of the atmosphere and temperature are required to achieve high quality ZnO growth at atmospheric pressure. Low energy consumption, low environmental load, simple configuration, low cost easy maintenance are among the advantages of a non-vacuum system. Fig. 1(a) is a schematic of the typical mist-CVD setup used in this investigation. This apparatus has two chambers, a mist vapor generator/atomizer (left) and a reaction chamber (right). Several different types of zinc precursors and solvents can be used for ZnO growth [9–11,17]. We used zinc acetate dehydrate ($Zn(CH_3COO)_2$) as the precursor, due to its smaller nucleation size and the resulting uniform surface morphology [17]. We used water as the solvent for its uniform precursor dissolution, straight-forward processing and non-toxic nature suitable for large scale production. The atomized mist was generated by a high-frequency ultrasonic resonator in the mist chamber and transferred to the reaction chamber. Simultaneously, the target substrate was heated to provoke mist vapor reaction on its surface. The gas phase of the vapor surrounding a mist droplet enables it to float on the heated substrate surface while maintaining slow evaporation as shown in Fig. 1b. In the steady state process, heat flux flows from the substrate to droplets and a mass flux of Zn^+ ions were transferred to the substrate surface. In the presence of atmospheric oxygen, a uniform layer of ZnO was formed on the substrate surface. Residual mist vapor incorporating CH_3COOH liquid droplet and carrier gas were pushed out of the chamber due to the higher chamber pressure compared to the ambient. Fig. 1c shows an atomic force microscopy (AFM) image of a typical ZnO film on glass substrate with an average thickness of 6.5 nm. Some ZnO particles (~5 nm) were observed on top of the ZnO film distributed randomly after the process. Thickness of the film was controlled precisely by growth time. Fig. 1d represents transmission spectra of ZnO films grown over different time periods. Previous investigations [18] verified that the observed transmission spectra closely approximated flat transmission over 1000 nm to 400 nm wavelength range, and decreased near UV. An increase in the ZnO film thickness dramatically increased the UV absorption while keeping unaltered transmission in visible range. A nearly flat transmission region at 330 nm was used to compare the transmittance of the ZnO growth time to film thickness. A 5 min growth results in transmittance of ~94.7% while a 32 min growth exhibits a 70.5% transmittance. These properties of the

ZnO films enable us to vary film thickness for appropriate electronic properties while maintaining high optical transmission. The relation between the transmittance and thickness (measured by AFM) is represented in Fig. 1e. A nearly linear trend in the transmittance (up to 70.5%) was observed with increasing ZnO film thickness. A 6 nm thick film resulted in 94.7% transmittance where as a 70.5% transmittance was obtained from a 30 nm thick ZnO film. A higher thickness of the film situated outside of this range could result nonlinearity in the transmittance vs thickness curve. However, we have observed a nearly linear transmittance vs thickness dependence until 30 nm thick ZnO films.

growth temperature up to 400 °C. Fig. 2c represents the SEM micrograph of the ZnO films grown at 400 °C. The ITO surface was not visible in this case due to the complete coverage of ZnO film. The ZnO particle size was observed on the order of 10 nm to 20 nm (see circle). The ZnO film surface morphology drastically changes beyond this growth temperature. Fig. 2d shows the SEM micrograph of the ZnO synthesis at 450 °C. Sharp conical shaped ZnO film morphology was observed in this case due to the fast growth rate at this temperature range (see highlighted circle). Fig. 2e illustrates the schematic summery of the ZnO growth process and corresponding surface morphology changes during different

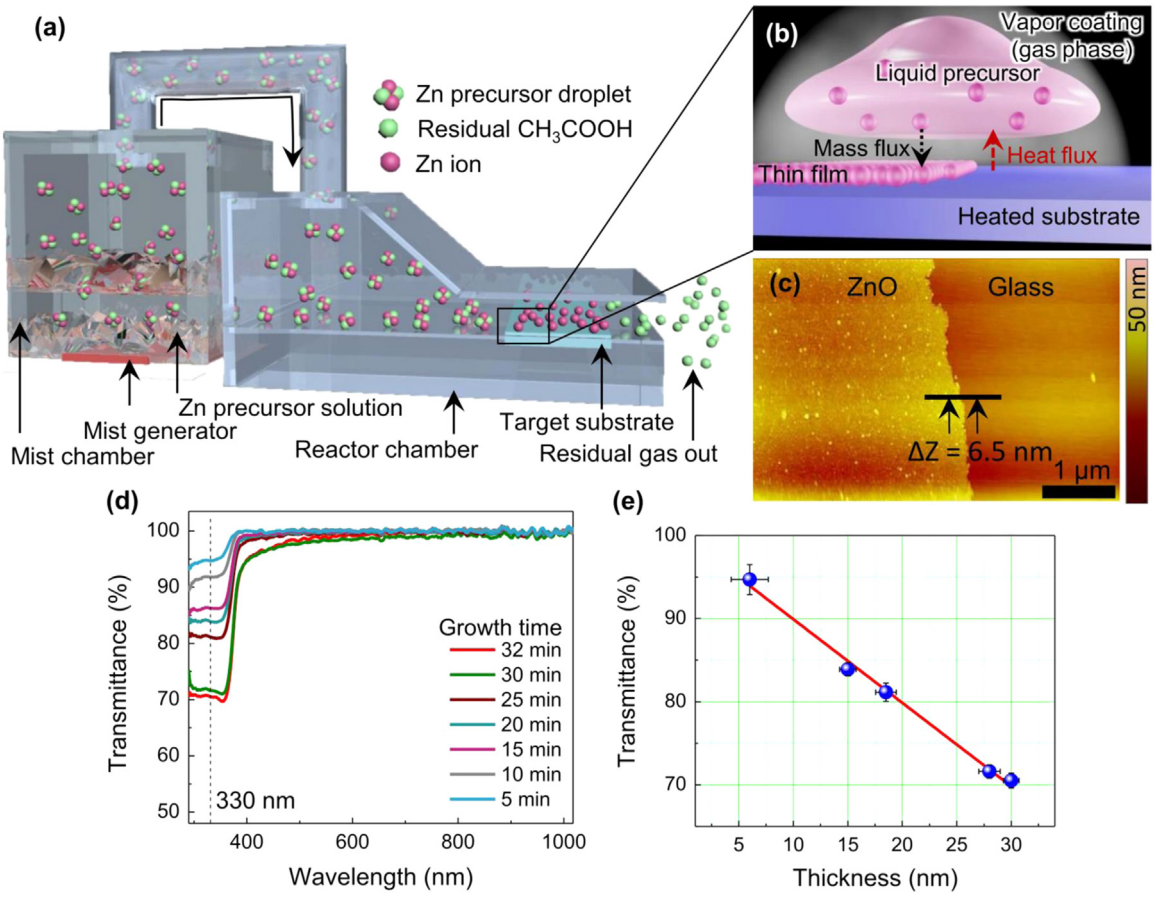

Fig. 1. (a) Schematic diagram of the mist-CVD system operated in the atmospheric pressure. This consists of a mist vapor generator/atomizer on the left and a reaction chamber on the right. The atomized mist was generated by a high-frequency ultrasonic resonator in the mist chamber and transferred to the reaction chamber in order to grow thin film. (b) Schematic illustration of a mist droplet containing liquid precursor surrounded by the mist vapor on top of the heated substrate. (c) AFM micrograph of the ZnO thin film deposited on top of a glass substrate. (d) Transmittance spectra of the mist-CVD grown ZnO film under different growth time. (e) Transmittance (at 330 nm wavelength) dependence of the mist-CVD grown ZnO thin film with different thickness.

Growth temperature can significantly alter the ZnO film quality in the above growth process. Different growth temperatures conditions were evaluated in order to understand ZnO synthesis process by mist-CVD method. Thin-film surface morphology grown under different growth temperature was characterized by scanning electron microscopy (SEM). Fig. 2 shows high resolution SEM micrographs of the ZnO films grown on indium tin oxide (ITO) substrate. A bare ITO substrate was demonstrated in Fig. 2a without ZnO coating. The ITO grain size was observed on the order of the 40 nm to 60 nm range (see arrow). Mist-CVD grown ZnO films synthesized at 250 °C resulted in a random distribution of small ZnO nanoparticles on the ITO substrate (see Fig. 2b) on the order of 5–6 nm (see arrow). ITO substrate morphology was still visible in this case due to a low ZnO coverage. In contrast, the substrate coverage can be significantly improved by rising the growth temperatures. The random ZnO particle distribution was observed at 250 °C as a result most of the ITO substrate remained uncovered. The ITO substrate was completely covered at 400 °C and a sharp conical shaped surface morphology was observed with 450 °C growth temperature.

An inverted polymer solar cell device was fabricated in order to investigate the optoelectronic properties of the above ZnO layers. ZnO thin films can be utilized as an optical spacer and electron conduction layer in the inverted polymer solar cell structure as described in reference [19–23]. Fig. 3a shows the schematic diagram of the inverted polymer solar cell (IPSC) device structure. Conventional IPSC devices are fabricated using glass/ITO/ZnO/P3HT:PCBM/MoO_3/Ag structure [24]. Conventional P3HT:PCBM based active layer has been extensively studied previously [25–28]. The optimized and deeply investigated active layer (P3HT:PCBM)

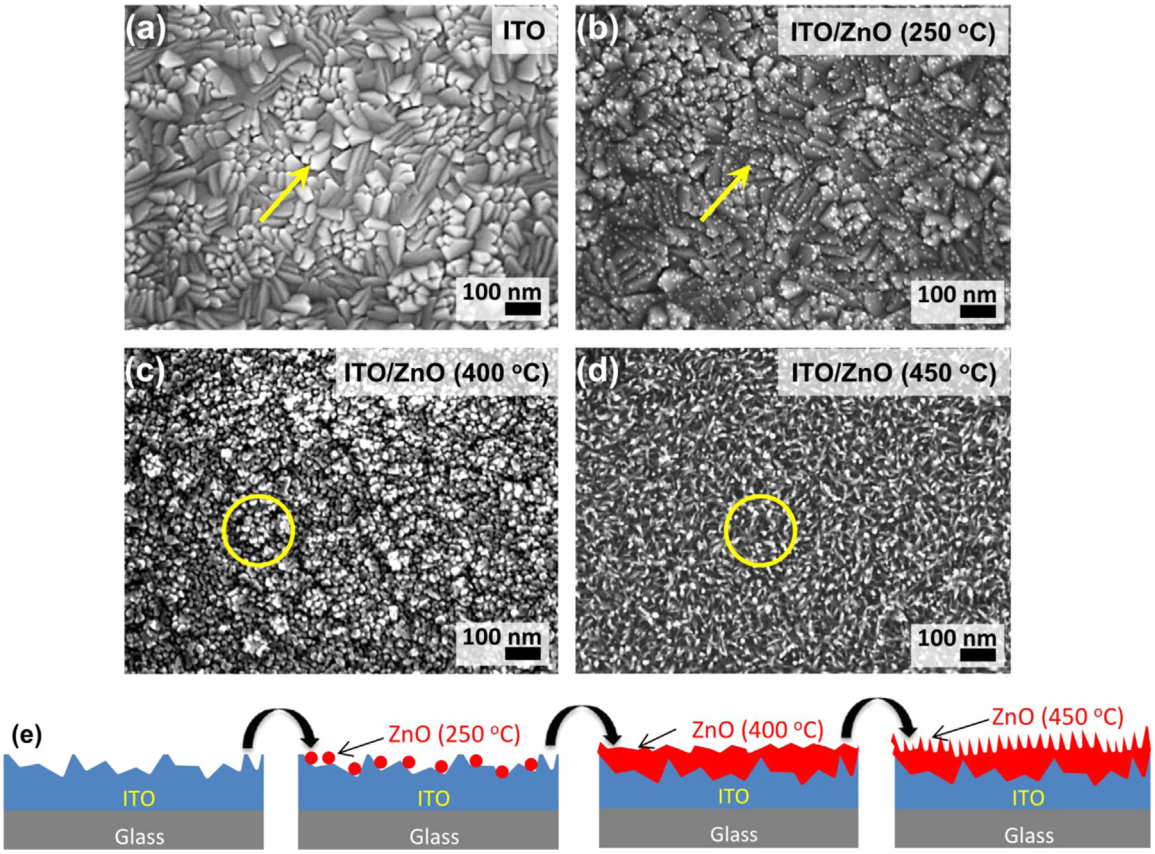

Fig. 2. (a–d) Scanning electron micrographs of a bare ITO substrate (a), and mist-CVD grown ZnO thin films (b–d) deposited on top the ITO at different growth temperatures. (e) Schematic diagram of the ZnO thin film growth process on top of a ITO substrate at different mist-CVD growth temperatures. Mist-CVD growth results in ZnO particle formation at 250 °C, the growth of continues thin films at 400 °C, and thin film shows a sharp conical shaped surface morphology around 450 °C.

was chosen to investigate the role of ZnO layers in the solar cell structure. Fig. 3b represents the I-V characteristics of the fabricated solar cells with the ZnO layer grown in different temperatures. The ZnO grown at 250 °C exhibits a low short circuit current density (J_{SC}) and an open circuit voltage (V_{OC}) with a solar cell power conversion efficiency (PCE) of 0.34%. J_{SC} and V_{OC} both can be improved drastically by increasing ZnO growth temperature up to 300 °C (PCE of 1.57%). A rise in the growth temperature up to 350 °C increases J_{SC} and V_{OC} further and results PCE up to 2.63%. An increment in the growth temperature further to 400 °C reduces the device J_{SC} and PCE consequently. The variations in PCE with the ZnO growth temperature was summarized in Fig. 3c. Small ZnO particles grown at low temperature of 250 °C (Fig. 2b) resulted poor devices performances with a 0.34% solar cell efficiency due to the low surface coverage. The coverage of the ZnO films becomes higher with increasing growth temperature as shown in Fig. 2b–d. This increases the consequent solar cell device efficiencies drastically. Maximum solar cell device efficiency (2.63%) was obtained from growth temperature near about 350 °C (shaded regions in the graph). A higher growth temperature results sharp conical shaped tips in ZnO films (Fig. 2d) and could be the key factor behind the decrease in J_{SC} (Fig. 3b) and PCE. The thickness of the ZnO films also plays a crucial role in the solar cell device performances (Fig. 3d). The ZnO film with a thickness between 5 nm and 20 nm (shaded region) resulted in maximum power conversion efficiencies of the solar cells. ZnO film thicknesses lower than 5 nm exhibited poor substrate coverage (demonstrated earlier) and low PCE. Increasing mist-CVD growth time from 5 min to 32 min resulted in thicker ZnO film (see Fig. S2a) and consequent transmittance of the film decreased from 92.7% to 70.5% as demonstrated in Fig. 1d–e respectively. Moreover, correspondingly highest J_{SC}, V_{OC}, FF, R_{Sh}, and R_S values were observed in the ZnO film thickness range between 5 nm and 20 nm (see Fig. S2b). The ZnO film thickness higher than 20 nm reduces the transmittance of the layer and consequent device PCE as demonstrated in Fig. 3e. A film transmittance range from 77% to 93% resulted high device efficiencies as demonstrated in the shaded regions in the graph.

As demonstrated in the previous section (Fig. 3), the ZnO film synthesized by mist-CVD method results rough surface morphology. The inverted polymer solar cell fabricated on top of this ZnO layer, results rough polymer-ZnO interface (Fig. 4a) and it could be the limiting factor for charge recombination and consequent low solar cell efficiencies. An uniform P3HT: PCBM active layer is critically important in order to reduce carrier recombination in high efficiency solar cells as demonstrated elsewhere [25–28]. A hybrid ZnO layer was synthesized in order to solve these issues combining the mist-CVD and sol-gel methods for high quality ZnO films. An inverted polymer solar cell was fabricated on top of this hybrid ZnO layer (see Fig. 4b). The primary use of the bi-layered hybrid ZnO layer was to enhance carrier conduction by a mist-CVD grown ZnO layer and reduction of carrier recombination using a uniform ZnO layer synthesized by a low temperature sol-gel method. The mist-CVD grown ZnO layer exhibits irregular surface morphology as compared to the sol-gel case, demonstrated by the SEM micrograph shown in Fig. 4c. The rough surface morphology of this ZnO film was reduced by depositing ZnO layer (30 nm) on top using sol-gel method. This sol-gel based ZnO in hybrid ZnO film resulted in smooth surface morphology (Fig. 4d) compare to mist-CVD based ZnO film (Fig. 4c). Furthermore, the smooth top surface morphology of hybrid ZnO film (Fig. 4d) facilitates uniform P3HT-PCBM film and reduces carrier recombination. The strategy of using a hybrid ZnO layer significantly increases the power

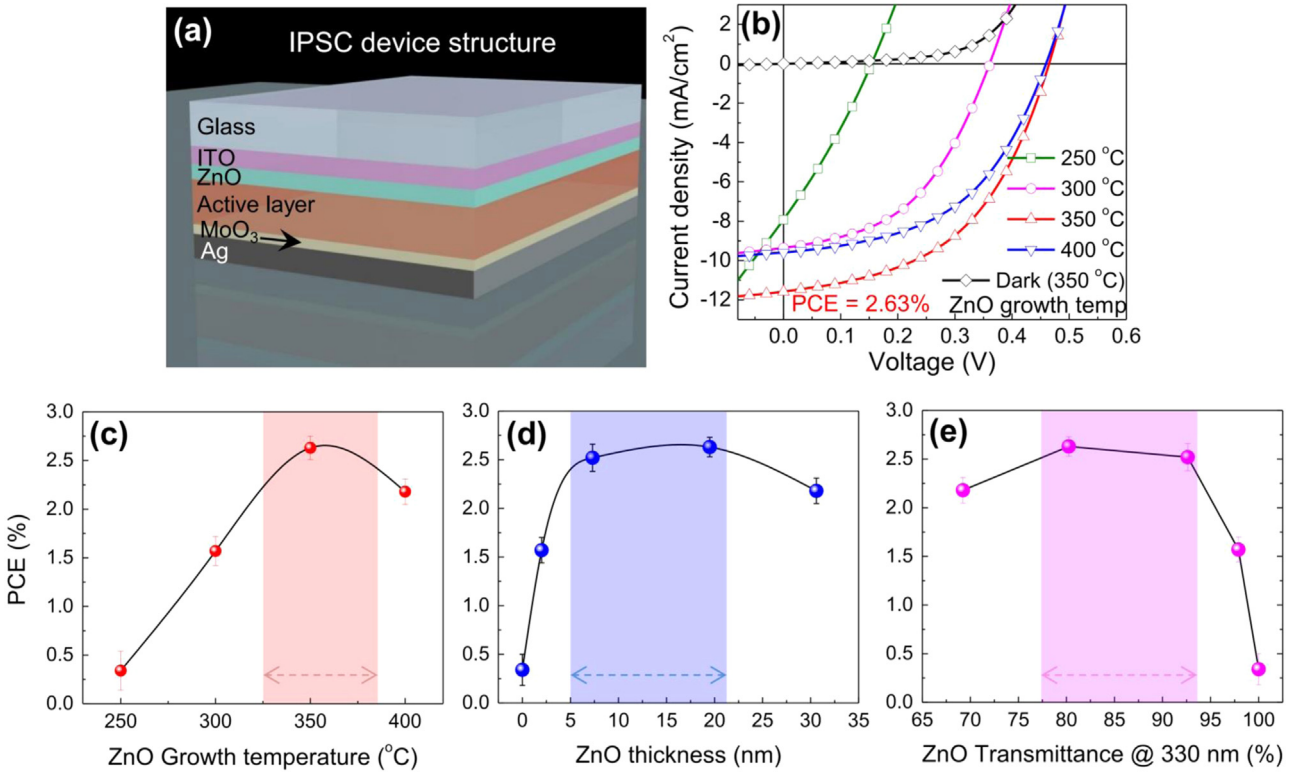

Fig. 3. (a) Schematic diagram of the inverted polymer solar cell structure containing glass/ITO/ZnO/P3HT:PCBM/MoO_3/Ag layers. (b) J-V characteristic of the inverted polymer solar cell devices containing different growth temperatures of the mist-CVD grown ZnO layer under dark and AM 1.5 solar irradiation. All other layers in the solar cell kept identical except for ZnO layers. (c) Variations in power conversion efficiencies of the IPSC for different mist-CVD growth temperatures. (d) PCE variations versus mist-CVD ZnO film thickness of the IPSC devices. (e) Dependence in power conversion efficiency versus the transmittance of mist-CVD ZnO layer (measured at $\lambda = 330$ nm). High solar cell efficiency was observed in the range (shaded regions) from 77% to 94% transmittance.

conversion efficiency of the solar cell devices (Fig. 4e). The PCE was limited to 2.6% and 3.1% by utilizing mist-CVD and sol-gel grown ZnO layers individually. However a hybrid ZnO layer exhibited very high solar cell power conversion efficiency up to 4.23%. These improvements were made possible by improving both J_{SC} and V_{OC} (see Fig. 4e) of the device due to the incorporation of hybrid ZnO layer. High quality hybrid ZnO layer was accomplished by varying growth temperature and film thickness as demonstrated in Fig. 4f and Fig. 4g, respectively. The power conversion efficiency of the solar cell containing hybrid ZnO layer was compared with mist-CVD grown devices under different growth temperatures. The hybrid ZnO exhibits highest PCE of 4.23% at around 350 °C growth temperature. Moreover, the power conversion efficiencies were significantly higher than simple mist-CVD samples (2.63%) as shown in Fig. 4f. Thickness variation also demonstrates a significant PCE improvement for the hybrid ZnO case compared with the mist-CVD grown ZnO film. The thickness of the sol-gel ZnO layer was kept constant at 30 nm while the mist-CVD layer thickness was varied for comparison (Fig. 4g). Both of the methods exhibit high PCE in the range of 10 nm to 15 nm ZnO layer thickness. However, a 64% improvement in PCE (4.23%) was observed for the hybrid ZnO in contrast of the mist-CVD devices (2.58%). High device current density (J_{SC}), open circuit voltage (V_{OC}), fill factor (FF), shunt resistance (R_{Sh}) and consequently low series resistance (R_S) are required for high power conversion efficiencies [24–28]. Fig. 4h shows the mist-CVD growth temperature variation of all the solar cell device parameters (J_{SC}, V_{OC}, FF, R_{Sh} and R_S). It was evident from the Fig. that the growth temperature near about 350 °C resulted high J_{SC} (11.98 mA/cm^2), V_{OC} (0.56 V), FF (0.63), R_{Sh} (1535 Ω/cm^2) and very low R_S (7 Ω/cm^2). These improvements resulted in high solar cell power conversion efficiencies for hybrid ZnO thin film. Deviation from this temperature range (350 °C) degrades solar cell parameters and consequent device efficiencies.

These improvements of the solar cell device parameters strongly highlight improved charge transport by the hybrid ZnO at around 350 °C. Charge transport mainly determined by the charge carrier drift across the device layers under applied electrical field. The magnitude of the carrier accumulation in the device can be readily determined by capacitance-voltage (C-V) and impedance spectroscopy [29–32]. In this study, the carrier concentration, charge mobility and carrier lifetime were obtained by the C-V measurement and impedance spectroscopy. These were conducted in order to investigate the charge transport properties across the device layers in dark and light conditions. First, Mott–Schottky curve and acceptor carrier concentration were measured using C-V measurements as demonstrated elsewhere [29–32]. Fig. 5a shows the measured capacitance (at frequency 1 kHz) as a function of the applied voltage. The magnitude of the oscillation signal amplitude was kept constant at 50 mV during the measurement. Inverted polymer solar cell devices can be modeled as a parallel plate capacitor during the C-V measurement [31,32]. The ITO and Ag electrodes can be considered as the top and bottom parallel plates separated by ZnO/P3HT:PCBM/MoO_3 in the middle. Both the P3HT:PCBM and MoO_3 were kept identical in all of the devices in order to evaluate changes driven by ZnO layers. The obtained device capacitance can be decomposed into two distinct regions as shown in Fig. 5a. i) Depletion layer modulated region (C_{dep}): where applied voltage (V) is less than built-in voltage (V_{bi}), ii) chemical capacitance region (C_μ): where capacitance is driven by $V > V_{bi}$ [30,32]. The minority carrier accumulation related chemical capacitance was measured under forward bias condition. The capacitance of the device remained nearly constant in C_{dep} region, however a sharp increase in the device capacitance was observed

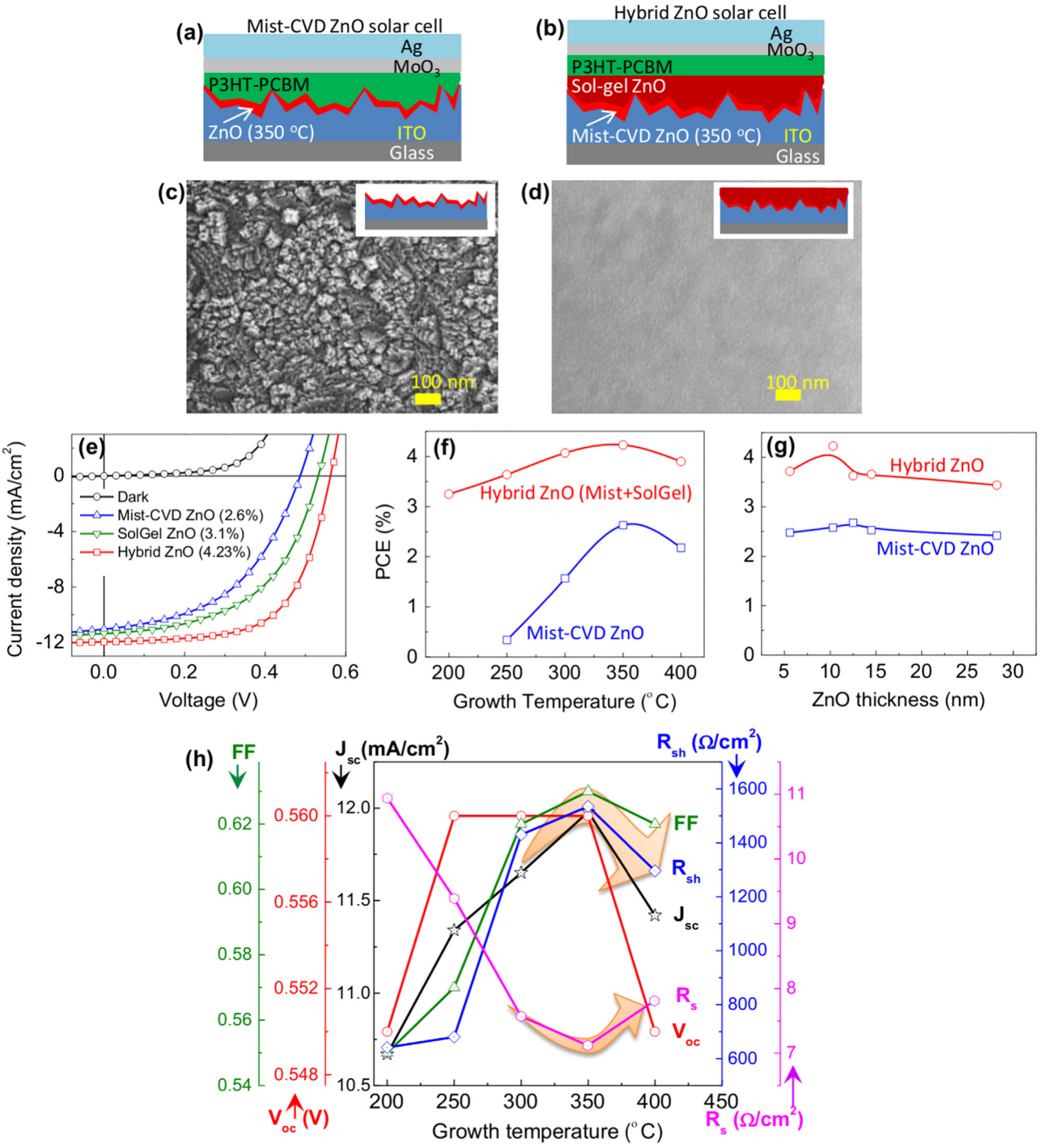

Fig. 4. (a) Schematic diagram of the inverted polymer solar cell with mist-CVD grown ZnO layer incorporating rough polymer interface. (b) IPSC device schematic diagram of smooth ZnO-polymer interface due to the hybrid ZnO layer. (c) SEM micrograph of the ZnO layer grown on top of the ITO substrate using the mist-CVD process. Inset shows the schematic diagram of the cross-section of this structure. (d) SEM micrograph of the hybrid ZnO layer grown on top of the ITO substrate highlights smooth ZnO-polymer interface. Inset shows the schematic of the cross-sectional view of the structure. (e) Comparisons between the J-V characteristics of IPSC devices containing hybrid ZnO, sol-gel ZnO and mist-CVD ZnO layers under AM 1.5 solar spectrum. Black circle curve represents the J-V characteristics of hybrid ZnO based solar cell in dark. (f, g) Comparisons between the PCE of hybrid ZnO and mist-CVD ZnO based IPSC with different mist-CVD growth temperatures (f), and mist-CVD grown ZnO thickness (g). Sol-gel ZnO growth temperature (200 °C) and thickness (30 nm) were kept constant during hybrid ZnO synthesis process in order to compare mist-CVD effects. (h) Multi Y axis plot of the hybrid ZnO inverted polymer solar cell device parameters with the mist-CVD growth temperature. Solar cell parameters from left to right: fill factor (FF), open circuit voltage (V_{OC}), current density (J_{SC}), shunt resistance (R_{Sh}) and series resistance (R_S) were represented.

under forward bias condition (C_μ region). Light illumination on the device showed a higher capacitance density, due to extra photo-generated charge carriers. The solar cell junction capacitance varies with bias dependent depletion layer modulation according to the Mott–Schottky relation [29–32]

$$C^{-2} = \frac{2(V_{bi}-V)}{A^2 e\varepsilon\varepsilon_0 N_A} \quad (1)$$

where, A is the device area, e is elementary charge, ε is the relative dielectric constant, ε_0 is the permittivity of the vacuum and N_A is the concentration of the acceptor impurities. The experimental

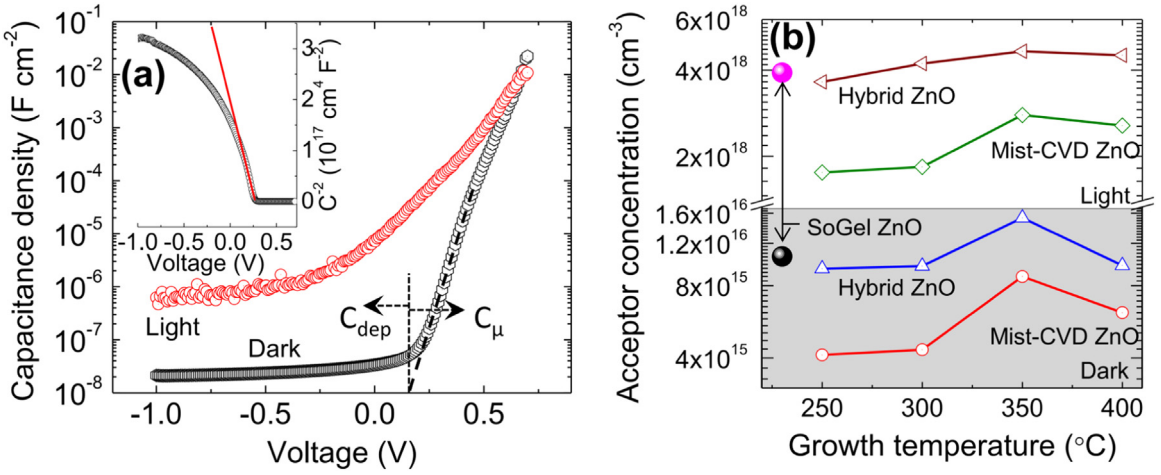

Fig. 5. (a) Capacitance density verses voltage characteristics of the hybrid ZnO based IPSC under dark and AM 1.5 solar irradiation. Inset represents the Mott–Schottky curve in dark condition derived from C-V measurement (black). (b) Variations in the acceptor concentrations versus mist-CVD growth temperatures for the sol-gel ZnO, hybrid ZnO and mist-CVD based solar cell devices. This compares the acceptor concentration and consequent efficiencies in the fabricated inverted polymer solar cell devices for different ZnO growth temperatures.

Mott–Schottky curve obtained from the IPSC devices was represented in the inset of Fig. 5a. Built in potential and acceptor concentration of the device can be calculated by fitting this curve using the above Eq. (1). The V_{bi} and N_A values was obtained as 0.27 V and 1.53×10^{16} cm^{-3}, respectively by using $\varepsilon = 3$ for 200 nm P3HT: PCBM layer [30]. This method enabled us to compare acceptor concentration of the hybrid ZnO with mist-CVD ZnO based solar cell devices. Fig. 5b demonstrates the variations in the acceptor carrier concentration versus ZnO growth temperature for different types of ZnO layers. It can be verified from the Fig. that the hybrid ZnO layer exhibits the highest (1.53×10^{16} cm^{-3}) acceptor concentration compared to the mist-CVD (8.7×10^{15} cm^{-3}) and sol-gel (1.05×10^{16} cm^{-3}) ZnO layers under dark condition. An overall increment in the effective acceptor concentration was observed in the solar cell under the light illumination condition due to photo-induced charge generation [32]. However, the highest acceptor carrier concentration trend in hybrid ZnO was maintained under light illumination. A gradual decrement in acceptor concentration was obtained with a ZnO growth temperature outside of the 350 °C range, both for dark and light conditions. This matches with the power conversion efficiency trend of the device obtained earlier (Fig. 4f). Therefore, a high acceptor carrier concentration was resulted from hybrid ZnO (grown near 350 °C) based devices. This plays a critical role behind improved solar cell device parameters and consequent PCE increments.

Moreover, carrier mobility and lifetime can be extracted using impedance spectroscopy measurements [30–32]. Conventional plots of the imaginary impedance (Z_{im}) and real impedance (Z_{re}) resulted in two eccentric semicircles for polymer solar cells as shown in previous literature [30–33]. Fig. 6a shows measured electrical impedance spectra of the hybrid ZnO IPSC in the complex plane under dark and light conditions. The device was measured under the open circuit condition and the oscillating frequency was varied from 40 Hz to 1 MHz while maintaining a

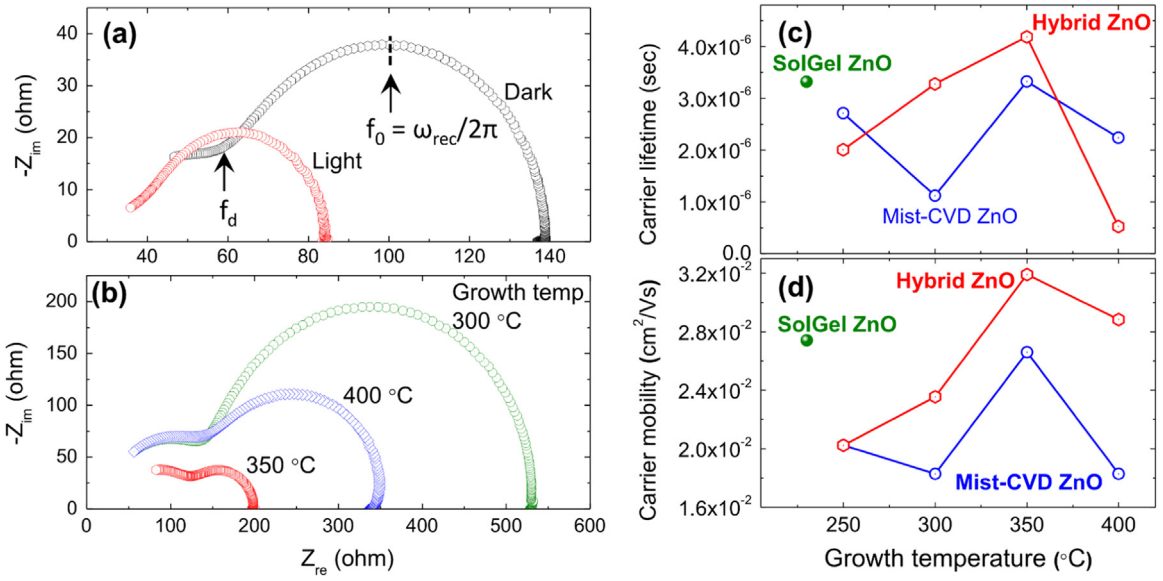

Fig. 6. (a) Impedance spectra of the hybrid ZnO based inverted polymer solar cell in dark and under AM 1.5 solar irradiation. (b) Comparisons in the impedance spectra between different growth temperatures of the hybrid ZnO based solar cells under dark condition. (c) Variations in the carrier lifetime with different mist-CVD growth temperatures were compared for the sol-gel ZnO, hybrid ZnO and mist-CVD ZnO based solar cell devices. (d) Carrier mobility as a function of the mist-CVD ZnO growth temperatures were compared for the same types of device as (c). High carrier lifetime and mobility and consequently high PCE (Fig. 4) were observed in hybrid ZnO based solar cells compare to non-hybrid ZnO devices.

constant amplitude of 50 mV. The impedance spectrum of the device under light illumination dramatically shifted the semicircle toward a lower resistance region (as shown in Fig. 6a) compared to the dark case. This could be resulted from the increments in charge carriers by photogeneration and corresponding decrement in the device resistance. The characteristic recombination frequency [32] (f_0 at max Z_{im}) was shifted from 98 Ω to 62 Ω under light compared to the dark condition. A similar behavior was observed from the hybrid ZnO layers grown under different growth temperatures (Fig. 6b). A high acceptor carrier concentration and low series resistance were obtained from the hybrid ZnO layer grown at 350 °C (Fig. 5). Fig. 6b verifies that a low f_0 could be due to high acceptor concentration and low series resistance in 350 °C (157 Ω) samples in comparison to the 400 °C (247 Ω) and 300 °C (337 Ω) growth temperatures. All the device layers were kept identical in order to compare the changes due to different ZnO layers. The impedance pattern reveals that the carrier transport could be determined by the diffusion–recombination between non-absorbing contacts [30]. The above result suggests that the improvements in the power conversion efficiencies could be triggered due to a higher acceptor carrier concentration and a low device resistance in the hybrid ZnO (grown at 350 °C) based solar cell devices. Furthermore, carrier lifetime and mobility of the devices were extracted from the impedance measurements. Carrier lifetime ($\tau_0=1/2\pi f_0$) can be directly calculated from the impedance spectroscopy using the characteristic recombination frequency (f_0) [29,30]. Fig. 6c demonstrates the carrier lifetime comparisons between different types of ZnO incorporated solar cell devices. The solar cell device with a hybrid ZnO layer grown at 350 °C exhibits a highest carrier lifetime (~4 μs) among other temperatures. The highest carrier lifetime (around 3.3 μs) from the mist-CVD and sol-gel ZnO devices was lower than that of hybrid ZnO case. Similarly the charge carrier mobility can be determined from the Nernst–Einstein relationship as $\mu_n=eD_n/K_BT$ [29–33]. Here D_n is the carrier diffusivity, and K_BT is the associated thermal energy. D_n can be calculated from the transition between the depletion layer driven impedance response and carrier diffusion–recombination associated impedance response at the diffusion frequency f_d ($D_n= f_d \times 2\pi eL^2$, where L is the active layer thickness ~200 nm). Fig. 6d represents the carrier mobility of the different types of ZnO incorporated solar cell devices. The hybrid ZnO solar cell exhibited the highest carrier mobility (0.032 cm^2/Vs) compared to the mist-CVD (0.026 cm^2/Vs) and sol-gel ZnO (27 cm^2/Vs) based solar cell devices. Moreover, hybrid ZnO based devices resulted in a highest carrier lifetime mobility and corresponding high device performances compared to non-hybrid ZnO. The above results strongly suggested that the increased acceptor carrier concentration, low device resistance, high carrier lifetime and mobility in the hybrid ZnO based solar cell devices play a critical role behind the improved power conversion efficiency.

4. Conclusions

A novel strategy to synthesize high quality hybrid ZnO thin films for improved inverted polymer solar cells was demonstrated. Hybrid ZnO thin films were synthesized by a simple, inexpensive approach with large scale synthesis compatibilities using a combination of mist-CVD and sol-gel processes. The precursor droplets introduced in mist-CVD to a well-defined temperature profile substrate results in high quality, large area hybrid ZnO films with nanoscale uniformity. The optimization of the hybrid ZnO layer was achieved in order to maximize solar cell carrier concentration, mobility and subsequent device efficiency. A 36% increase in solar cell device efficiency up to 4.23% was demonstrated using the hybrid ZnO layer as compared to non-hybrid ZnO devices (3.1%). The hybrid ZnO film with the mist-CVD growth temperature near about 350 °C and film thickness in the range of 5 nm to 20 nm exhibited high efficiency inverted polymer solar cells. Deviation from this range resulted poor ZnO film coverage, highly non-uniform surface morphology, and poor solar cell performances. The hybrid ZnO based inverted polymer solar resulted high carrier concentration and power conversion efficiencies compared to the mist-CVD and sol-gel based ZnO. Furthermore, our results strongly suggested that the increased carrier concentration, low device resistance, high carrier lifetime and high mobility in hybrid ZnO based solar cell devices could be the reason behind the high power conversion efficiencies compared to conventional non-hybrid ZnO structures. Since ZnO thin film is a heavily used material for a broad range of solar cell applications (such as organic polymer solar cell, dye sensitized solar cell, quantum dot solar cell) therefore, the utilization of the hybrid ZnO films show a potential to improve solar cell efficiency by replacing todays non-hybrid ZnO materials.

Acknowledgments

We would like to acknowledge the collaboration of this research with King Abdul-Aziz City for Science and Technology (KACST) via The Center of Excellence for Green Nanotechnologies (CEGN). Authors acknowledge Dr. M. A. Zurbuchen for the manuscript editing in some sections.

Appendix A. Supporting information

Supplementary data associated with this article can be found in the online version at http://dx.doi.org/10.1016/j.solmat.2016.08.022.

References

[1] E. Fortunato, P. Barquinha, R. Martins, Oxide semiconductor thin-film transistors: a review of recent advances, Adv. Mater. 24 (2012) 2945–2986.
[2] J.L. Zhao, X.M. Li, J.M. Bian, W.D. Yu, X.D. Gao, Structural, optical and electrical properties of ZnO films grown by pulsed laser deposition (PLD), J. Cryst. Growth 276 (2005) 507–512.
[3] M.-C. Jeong, B.-Y. Oh, W. Lee, J.-M. Myoung, Comparative study on the growth characteristics of ZnO nanowires and thin films by metalorganic chemical vapor deposition (MOCVD), J. Cryst. Growth 268 (2004) 149–154.
[4] H. Ju, Ko, Y. Chen, S. Ku Hong, T. Yao, MBE growth of high-quality ZnO films on *epi*-GaN, J. Cryst. Growth 209 (2000) 816–821.
[5] E. Ohshima, H. Ogino, I. Niikura, K. Maeda, M. Sato, M. Ito, T. Fukuda, Growth of the 2-in-size bulk ZnO single crystals by the hydrothermal method, J. Cryst. Growth 260 (2004) 166–170.
[6] Y. Natsume, H. Sakata, Zinc oxide films prepared by sol-gel spin-coating, Thin Solid Films 372 (2000) 30–36.
[7] D. Gal, G. Hodes, D. Lincot, H.W. Schock, Electrochemical deposition of zinc oxide films from non-aqueous solution: a new buffer/window process for thin film solar cells, Thin Solid Films 361–362 (2000) 79–83.
[8] T. Kawaharamura, Physics on development of open-air atmospheric pressure thin film fabrication technique using mist droplets: control of precursor flow, Jpn. J. Appl. Phys. 53 (2014) 05FF08.
[9] X. Zhu, T. Kawaharamura, A.Z. Stieg, C. Biswas, L. Li, Z. Ma, M.A. Zurbuchen, Q. Pei, K.L. Wang, Atmospheric and aqueous deposition of polycrystalline metal oxides using Mist-CVD for highly efficient inverted polymer solar cells, Nano Lett. 15 (2015) 4948–4954.
[10] K.-S. Shin, H.-J. Park, B. Kumar, K.-K. Kim, S.-G. Ihn, S.-W. Kim, Low-temperature growth and characterization of ZnO thin films for flexible inverted organic solar cells, J. Mater. Chem. 21 (2011) 12274–12279.
[11] G.T. Dang, T. Kawaharamura, M. Furuta, S. Saxena, M.W. Allen, Stability of In-Ga-Zn-O metal-semiconductor field-effect-transistors under bias, illumination, and temperature stress, Appl. Phys. Lett. 107 (2015) 143504.
[12] T. Kawaharamura, T. Hirao, Development and research on the mechanism of novel mist etching method for oxide thin films, Jpn. J. Appl. Phys. 51 (2012) 036503.
[13] G.T. Dang, T. Kawaharamura, M. Furuta, M.W. Allen, Metal-semiconductor field-effect transistors with in #x2013;Ga #x2013;Zn #x2013;O channel

grown by nonvacuum-processed mist chemical vapor deposition, IEEE Electron Device Lett. 36 (2015) 463–465.
[14] T. Kawaharamura, H. Nishinaka, S. Fujita, Growth of crystalline zinc oxide thin films by fine-channel-mist chemical vapor deposition, Jpn. J. Appl. Phys. 47 (2008) 4669–4675.
[15] Y. Sun, J.H. Seo, C.J. Takacs, J. Seifter, A.J. Heeger, Inverted polymer solar cells integrated with a low-temperature-annealed sol-gel-derived ZnO film as an electron transport layer, Adv. Mater. 23 (2011) 1679–1683.
[16] H.-L. Yip, S.K. Hau, N.S. Baek, H. Ma, A.K.Y. Jen, Polymer solar cells that use self-assembled-monolayer- modified ZnO/metals as cathodes, Adv. Mater. 20 (2008) 2376–2382.
[17] C. Biswas, Z. Ma, X. Zhu, T. Kawaharamura, K.L. Wang, Inverted polymer solar cells based on thin ZnO films grown by Mist chemical vapor deposition system, SPIE Optics+Photonics Proceedings, 9184, 2014, pp. 57.
[18] S.T. Tan, B.J. Chen, X.W. Sun, W.J. Fan, H.S. Kwok, X.H. Zhang, S.J. Chua, Blueshift of optical band gap in ZnO thin films grown by metal-organic chemical-vapor deposition, J. Appl. Phys. 98 (2005) 013505.
[19] S.K. Hau, H.-L. Yip, N.S. Baek, J. Zou, K. O'Malley, A.K.Y. Jen, Air-stable inverted flexible polymer solar cells using zinc oxide nanoparticles as an electron selective layer, Appl. Phys. Lett. 92 (2008) 253301.
[20] F.C. Krebs, S.A. Gevorgyan, J. Alstrup, A roll-to-roll process to flexible polymer solar cells: model studies, manufacture and operational stability studies, J. Mater. Chem. 19 (2009) 5442–5451.
[21] S.K. Hau, H.-L. Yip, H. Ma, A.K.Y. Jen, High performance ambient processed inverted polymer solar cells through interfacial modification with a fullerene self-assembled monolayer, Appl. Phys. Lett. 93 (2008) 233304.
[22] K. Norrman, M.V. Madsen, S.A. Gevorgyan, F.C. Krebs, Degradation patterns in water and oxygen of an inverted polymer solar cell, J. Am. Chem. Soc. 132 (2010) 16883–16892.
[23] J.-S. Huang, C.-Y. Chou, M.-Y. Liu, K.-H. Tsai, W.-H. Lin, C.-F. Lin, Solution-processed vanadium oxide as an anode interlayer for inverted polymer solar cells hybridized with ZnO nanorods, Org. Electron. 10 (2009) 1060–1065.
[24] A.K.K. Kyaw, X.W. Sun, C.Y. Jiang, G.Q. Lo, D.W. Zhao, D.L. Kwong, An inverted organic solar cell employing a sol-gel derived ZnO electron selective layer and thermal evaporated MoO3 hole selective layer, Appl. Phys. Lett. 93 (2008) 221107.
[25] C.J. Brabec, S. Gowrisanker, J.J.M. Halls, D. Laird, S. Jia, S.P. Williams, Polymer–Fullerene bulk-heterojunction solar cells, Adv. Mater. 22 (2010) 3839–3856.
[26] H. Wang, M. Shah, V. Ganesan, M.L. Chabinyc, Y.-L. Loo, Tail State-assisted charge injection and recombination at the electron-collecting interface of P3HT: PCBM bulk-heterojunction polymer solar cells, Adv. Energy Mater. 2 (2012) 1447–1455.
[27] H. Chen, S. Hu, H. Zang, B. Hu, M. Dadmun, Precise structural development and its correlation to function in conjugated polymer: fullerene thin films by controlled solvent annealing, Adv. Funct. Mater. 23 (2013) 1701–1710.
[28] N.D. Treat, M.A. Brady, G. Smith, M.F. Toney, E.J. Kramer, C.J. Hawker, M. L. Chabinyc, Interdiffusion of PCBM and P3HT reveals miscibility in a photovoltaically Active Blend, Adv. Energy Mater. 1 (2011) 82–89.
[29] G. Garcia-Belmonte, P.P. Boix, J. Bisquert, M. Sessolo, H.J. Bolink, Simultaneous determination of carrier lifetime and electron density-of-states in P3HT:PCBM organic solar cells under illumination by impedance spectroscopy, Sol. Energy Mater. Sol. Cells 94 (2010) 366–375.
[30] G. Garcia-Belmonte, A. Munar, E.M. Barea, J. Bisquert, I. Ugarte, R. Pacios, Charge carrier mobility and lifetime of organic bulk heterojunctions analyzed by impedance spectroscopy, Org. Electron. 9 (2008) 847–851.
[31] F. Fabregat-Santiago, G. Garcia-Belmonte, I. Mora-Seró, J. Bisquert, Characterization of nanostructured hybrid and organic solar cells by impedance spectroscopy, Phys. Chem. Chem. Phys. 13 (2011) 9083–9118.
[32] J. Bisquert, F. Fabregat-Santiago, I. Mora-Seró, G. Garcia-Belmonte, S. Giménez, Electron lifetime in dye-sensitized solar cells: theory and interpretation of measurements, J. Phys. Chem. C 113 (2009) 17278–17290.
[33] T. Kuwabara, Y. Kawahara, T. Yamaguchi, K. Takahashi, Characterization of inverted-type organic solar cells with a ZnO layer as the electron collection electrode by ac impedance spectroscopy, ACS Appl. Mater. Interfaces, 1, (2009) 2107–2110.